

<https://doi.org/10.1038/s42003-025-07876-5>

Longitudinal excitation-inhibition balance altered by sex and *APOE*- ϵ 4



Andrew P. Burns¹ , Igor Fortel¹, Liang Zhan², Orly Lazarov³, R. Scott Mackin^{4,5}, Alexander P. Demos⁶, Barbara Bendlin^{7,8} & Alex Leow¹ 

Neuronal hyperexcitation affects memory and neural processing across the Alzheimer's disease (AD) cognitive continuum. Levetiracetam, an antiepileptic, shows promise in improving cognitive impairment by restoring the neural excitation/inhibition balance in AD patients. We previously identified a hyper-excitable phenotype in cognitively unimpaired female *APOE*- ϵ 4 carriers relative to male counterparts cross-sectionally. This sex difference lacks longitudinal validation; however, clarifying the vulnerability of female ϵ 4-carriers could better inform antiepileptic treatment efficacy. Here, we investigated this sex-by- ϵ 4 interaction using a longitudinal design. We used resting-state fMRI and diffusion tensor imaging collected longitudinally from 106 participants who were cognitively unimpaired for at least one scan event but may have been assessed to have clinical dementia ratings corresponding to early mild cognitive impairment over time. By including scan events where participants transitioned to mild cognitive impairment, we modeled the trajectory of the whole-brain excitation-inhibition ratio throughout the preclinical cognitively healthy continuum and extended to early impairment. A linear mixed model revealed a significant three-way interaction among sex, ϵ 4-status, and time, with female ϵ 4-carriers showing a significant hyper-excitable trajectory. These findings suggest a possible pathway for preventative therapy targeting preclinical hyperexcitation in female ϵ 4-carriers.

The balance of neural excitation-inhibition (E/I) is crucial for brain functions like memory formation^{1,2} and retrieval³ and is altered in neurodegenerative diseases such as Alzheimer's disease (AD). Meta-analyses show that E/I imbalances, including subclinical epileptiform activity (SEA) and seizures, are linked to impaired cognition and faster cognitive decline in AD patients^{4–10}. Follow-up cohort studies using fMRI, electroencephalography (EEG), or magnetoencephalography (MEG) comparing memory-encoding tasks and resting-state activity between different groups such as AD-dementia, mild cognitive impairment (MCI), offspring of AD patients, and cognitively unimpaired individuals support the theory the presymptomatic hyperexcitation (Fig. 1) in cognitively unimpaired individuals that continues into, and perhaps peaks, in early MCI^{11–20}. Regionally, this increase of activity has primarily been observed in the hippocampus and entorhinal cortex, central structures in memory consolidation and AD. Many of these

same studies find distinct EEG/MEG frequency-band specific E/I changes in cognitively unimpaired, MCI, and AD-dementia (e.g. increase of theta band power during cognitive decline) that substantiates the connection of E/I imbalances to cognitive status^{11,16–22}. Fig. 1 shows a provisional order of events originally proposed and illustrated by Koelewijn et al., attempting to provide a unifying early hyperexcitation theory as well as late hypoactivity and hypoconnectivity for dozens of mouse and human studies. Still, more comprehensive and robust studies are needed to verify this schematic order of events, as they have recognized conflicting study results¹⁶. Several review articles have extensively covered this theory, as well as its advantages and limitations in summarizing current results from mouse and human studies that we refer the reader to for a more comprehensive validation^{19,23–33}.

Further corroborating the relationship between E/I imbalances and AD protein pathology, amyloid plaques^{11,34–39} and tau^{11,35,40–42} have been

¹Department of Biomedical Engineering University of Illinois Chicago (UIC), 851 S Morgan St, Chicago, IL, 60607, USA. ²Department of Electrical and Computer Engineering, University of Pittsburgh, 4200 Fifth Avenue, Pittsburgh, PA, 15260, USA. ³Department of Anatomy and Cell Biology, College of Medicine, University of Illinois Chicago, 808 S. Wood St, Chicago, IL, 60612, USA. ⁴Department of Psychiatry and Behavioral Sciences, University of California San Francisco, 675 18th St, San Francisco, CA, 94107, USA. ⁵Department of Veterans Affairs Medical Center, 4150 Clement Street, San Francisco, CA, USA. ⁶Department of Psychology, University of Illinois Chicago (UIC), 1007 W Harrison St, Chicago, IL, 60607, USA. ⁷Department of Medicine, University of Wisconsin-Madison, 5158 Medical Foundation Centennial Building, 1685 Highland Ave, Madison, WI, 53792, USA. ⁸Wisconsin Alzheimer's Disease Research Center, University of Wisconsin-Madison, 600 Highland Ave J5/1 Mezzanine, Madison, WI, 53792, USA. ✉e-mail: drew4495@gmail.com; alexleow@alumni.ucla.edu

shown to be associated with and cause hyperexcitable and hypo-excitable changes, respectively. However, some research suggests that neuronal hyperactivity and E/I imbalances could precede amyloid plaque deposition, causing a vicious positive feedback cycle between E/I changes and AD protein pathology, though this is not fully established^{34,38,43–51}. For instance, studies in transgenic mice have observed hyperexcitable neuronal activity before and independent of amyloid plaque formation^{34,38,49}. Additionally, hyperexcitation and altered synaptic activity has been observed to modulate the amount of amyloid-beta (A β) that accumulates in plaques in a region-dependent manner^{46–52}. For example, Yamamoto et al. demonstrated that chronic optogenetic activation of neurons in an APP transgenic mouse model increased local A β burden by approximately 2.5-fold compared to controls⁵². Similarly, Yuan et al. showed that reducing neural activity (chemogenetically) decreased A β aggregation while increasing neural activity enhanced amyloid plaque deposition, suggesting that attenuation of neural activity could be a viable therapeutic approach for AD⁴⁷. However, these findings are primarily from animal models, and further research is needed to confirm whether similar mechanisms occur in humans.

Despite the direct epidemiological and neuroimaging evidence of E/I imbalances throughout the continuum of AD and the connection of altered E/I with AD neuropathological proteins, amyloid and tau, E/I has not been comprehensively investigated with other AD risk factors and

pathophysiology. Perhaps most prominently, females, particularly those with genetic *APOE*- ϵ 4 allele, have double the risk of developing AD dementia^{53,54}. Given that female sex is a recognized risk factor with unexplained pathophysiological differences in AD, investigating E/I imbalances differentiated by sex is crucial, and will inform the growing interest in early intervention with antiepileptic therapies, such as levetiracetam^{10,55–61}.

In this study, we evaluate the relationship between sex and *APOE*- ϵ 4 on longitudinal E/I balance changes in 106 cognitively unimpaired older adults using a multi-modal connectomics approach^{62,63}. Using both functional (fMRI) and structural connectivity (diffusion-weighted imaging) for each participant, we estimated a whole-brain excitation-inhibition ratio (EIR) that captures both functional and structural connectivity brain dynamics. This multimodal approach is advantageous over most other methods that rely solely on functional data, which may inadequately reconstruct excitation dynamics. Using each participant's unique EIR in a linear mixed model, we show that *APOE*-specific preclinical hyperexcitation is also female-specific. This work is the first-time demonstrating sex-specific hyperexcitation in human longitudinal studies and aims to support novel E/I-based treatment approaches to reduce dementia risk by addressing these sex-specific imbalances.

Results
Patient demographics and descriptive statistics

Our primary model included participants meeting longitudinal criteria, and sub-analyses included more limited subsets of participants with amyloid PET imaging (Table 1). While we note several disproportionalities between groups or scan events below, it is important to note that while these imbalances affect sensitivity and generalizability of our model, it does not greatly impact the bias our linear mixed model. Mixed effect modeling is well-suited for handling unbalanced data, and the inclusion of the imbalanced groups as covariates ensures our estimates remain unbiased. Sample sizes per sex and ϵ 4-carrier status were adequate but skewed towards females to males (65: 41) and non- ϵ 4 to ϵ 4-carrying (77: 29) participants. Most participants (95%) had three or four scan events; one had six. Given the above, each group had sufficient counts for a mixed modeling. However, a drastic decrease in ϵ 4 representation resulted when including amyloid PET status (45 non- ϵ 4 : 15 ϵ 4) or restricting to only amyloid-negative participants (37 non- ϵ 4 : 6 ϵ 4). Therefore, we labeled these as exploratory sub-analyses due to limited generalizability. Age was equally represented between ϵ 4-carrier groups. Nearly all participants were cognitively unimpaired out of 349 total scan combinations (324 with CDR=0, 21 with CDR=0.5, and 1 with CDR=1). We included 22 participants with CDR values greater than 0 since they all had at least one scan event with a CDR=0, and we wanted to model the trajectory of neural excitation-inhibition throughout the preclinical cognitive continuum up until early mild cognitive impairment. Additional reasons for the inclusion of these participants

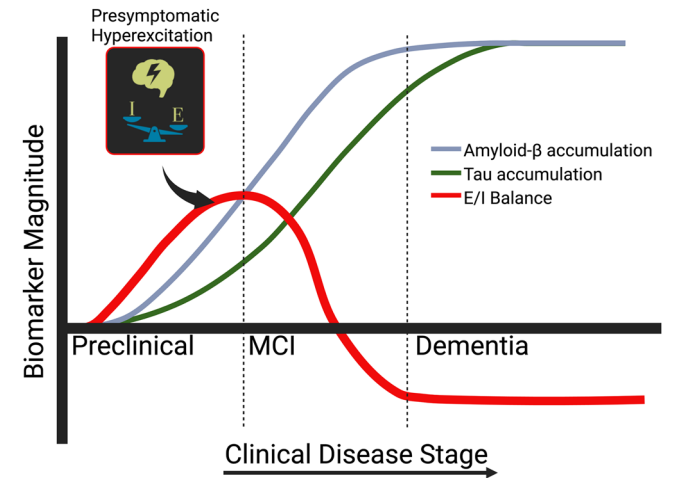


Fig. 1 | Hypothesized time course of excitation-inhibition balance in AD-related decline. Schematic representation of a speculated excitation-inhibition (E/I) order of events during the course of Alzheimer’s disease (preclinical, MCI, and dementia) and associated protein pathologies (amyloid- β and tau). This representation was proposed by Koelewijn et al., based on converging preliminary studies. Created in BioRender. Duran, M. (2025) <https://BioRender.com/d70o684>.

Table 1 | Subject demographics

	All Subjects		Amyloid PET		Amyloid Negative	
	ϵ 4 carriers	non- ϵ 4 carriers	ϵ 4 carriers	non- ϵ 4 carriers	ϵ 4 carriers	non- ϵ 4 carriers
Total # (scans: subjects)	89:29	257:77	45:15	146:45	18:6	117:37
Sex (M:F)	10:19	31:46	5:10	20:25	3:3	14:23
Age (years:standard deviation)	70.1:8.6	68.3:9	67.8:7	68.5:8.2	65.1:6.2	68:8.9
Number of individual scans (3:4:5:6)	27:2:0:0	57:15:4:1	15:0:0:0	35:9:1:0	6:0:0:0	31:6:0:0
CDR by scan (0:0.5:1)	84:5:0	240:16:1	42:3:0	139:7:0	16:2:0	116:1:0

Colons separate values labels in row titles. “Number of individual scans” and “CDR by scan” represent value counts for values specified in row titles.

were due to CDR measurement variability between physicians and it is common for participants to be assessed as CDR = 0.5, to only return to CDR = 0 in the next scan event. Therefore, to truly model the preclinical continuum, it is justified to incorporate these participants, since not only do they possess scan events with a CDR = 0, but there is strong rationale to suggest that CDRs of 0.5 could be transient periods of impairment during the preclinical period or false positives. A comprehensive count breakdown of number of CDR measurements per participant is seen in Supplementary Table 13.

Interaction between sex and *APOE*- $\epsilon 4$ modulates whole-brain excitation trajectory

Using each participant's unique rsSC-derived whole-brain EIR, we tested the hypothesis that EIR trajectory is altered by sex and *APOE*- $\epsilon 4$ status. The EIR, the ratio of summed positive (excitatory) to negative (inhibitory) edges in the simulated hybrid connectome (rsSC), was regressed against sex, $\epsilon 4$ status, time since first scan (in years), and age at first scan, with random effects accounting for repeated measures. The reference group was female and *APOE*- $\epsilon 4$ negative. All model results and omnibus F-tests are reported in Supplementary Tables 1–12. Each statistical test result is reported below with its associated unstandardized (sex and $\epsilon 4$ status) or semi-standardized coefficients (time since first scan and age at first scan were scaled: centered and divided by its standard deviation) for effect size (b).

Whole-brain EIR showed a significant three-way interaction between time since first scan, sex, and $\epsilon 4$ status ($b = -0.045$, $p = 0.018$). Visualization (Fig. 2) and a significant simple two-way interaction within each sex (i.e., time since first scan by $\epsilon 4$ status) showed that females are driving this three-way interaction ($b = 0.022$, $p = 0.042$) as males did not show the same pattern ($b = -0.023$, $p = 0.144$). Additional pairwise comparisons to unpack the significant simple two-way interaction showed a significantly higher hyperexcitable trajectory (slope) risk for $\epsilon 4$ -positive females compared to $\epsilon 4$ -negative females ($b = 0.009$, $p = 0.042$). Further, $\epsilon 4$ -positive females showed a near-significant hyperexcitable risk, with a larger slope, compared to $\epsilon 4$ -positive males ($b = 0.013$, $p = 0.052$). In further support of the sex-*APOE* effect, female's hyperexcitable trajectory in the years after their first scan was moderated by the age at which they entered the study ($b = 0.026$, $p = 0.015$). A simple slopes analysis (-1 SD vs 1 SD age at first scan) revealed that older females at the start of the study showed a larger EIR trajectory difference between $\epsilon 4$ -negative and $\epsilon 4$ -positive (75.2 years, $b = -0.019$, $p = 0.007$), than those who started younger (58.5 years, $b = 0.001$, $p = 0.78$). Given the current understanding of global whole-brain hyperexcitation being a gradual long-term change, closer inspection of individual trajectories (Supplementary Fig. 1) revealed two high-leverage participants with data spanning over 7.5 years. As expected, a sensitivity analysis removing these participants shifted the p -values, but the patterns remained the same with a similar effect size for the three-way interaction ($b = -0.032$, $p = 0.086$).

To ensure the robustness of the dependent variable and test amyloid as a confounder, we conducted four sub-analysis models: 1) replacing EIR with an alternative definition of excitation-inhibition (excitation percentage), 2) amyloid-negative participants only, 3) amyloid as a non-interacting covariate, and 4) amyloid as an interacting covariate. Replacing EIR with excitation percentage (1) did not appreciably change model results or significance. Neither amyloid-negative (2) models nor binary amyloid status as an interacting covariate (4) showed significant effects. However, including amyloid status as a non-interacting term (3) reduced model complexity (31 to 16 fixed-effect terms compared to amyloid as an interacting predictor) and maintained significance of the main model's: 1) two-way interaction between time since first scan and $\epsilon 4$ status for females ($b = 0.031$, $p = 0.028$), and 2) three-way interaction between time since first scan, sex, and $\epsilon 4$ status ($b = -0.057$, $p = 0.020$). These models suggest robustness of the significant effects despite potential amyloid influence.

Female-specific hyperexcitation in the default mode network

Given that EIR is a graph metric, it allows one to probe regional and network-based analysis. However, due to the constraints of mapping functional activity onto empirical connectivity coefficients and the necessity for multiple comparison corrections across regions/networks, regional and network-based analyses are inherently noisier and have lower statistical power. Due to this constraint, we conducted a strictly hypothesis-driven functional network analysis. Specifically, functional network differences in Alzheimer's disease have been consistently reported in the default mode network (DMN)^{64–71} and limbic system^{72,73}, with some highlighting the salience network. While the nascent field of functional network disruptions in AD and MCI is not heavily standardized and there is currently a lack of reporting for negative findings, the DMN and limbic systems are two of the most consistent and ubiquitously reported networks, with the DMN dominating attention, as shown in Badhwar et al.'s systematic review and meta-analysis of Alzheimer's disease literature⁷². Due to this heavy literature skew and evidence, as well as the ROIs in the DMN and limbic system having a clear theoretical connection to structures (e.g., hippocampus, middle temporal gyrus) and cognitive abilities (e.g., memory, emotional regulation) implicated in Alzheimer's disease neuropathology and symptomatology, we limited our network analysis to an aggregate of both the DMN and limbic networks.

Using the same linear mixed model approach described above, we next tested the hypothesis that cognitively unimpaired females show elevated excitatory activity in the DMN and limbic system compared to males. The regions defining this aggregate network are the middle temporal gyrus, frontal medial cortex, subcallosal cortex, angular gyrus, cingulate gyrus (posterior division), precuneus cortex, parahippocampal gyrus (anterior division), temporal fusiform cortex, hippocampus, and amygdala and are based on the functional annotations accompanying the ROI parcellations specified in "Methods" and "Supplementary material." Results from the

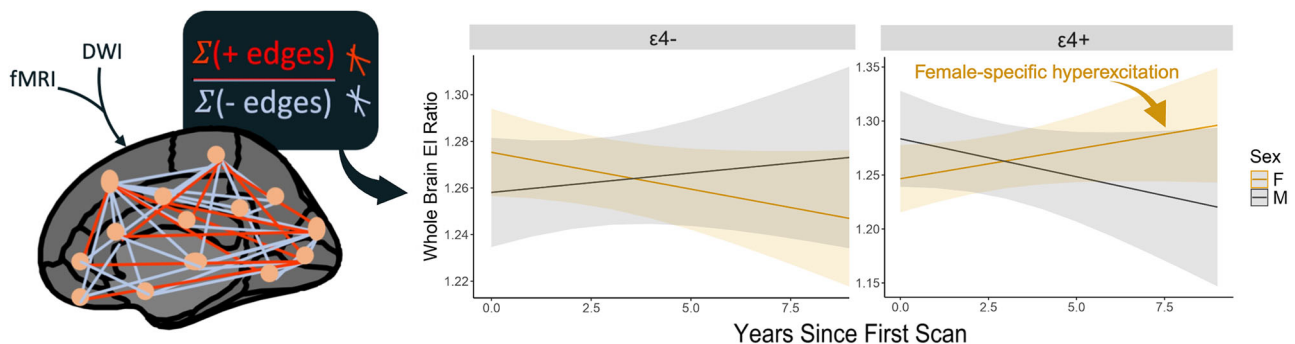


Fig. 2 | Sex and *APOE*- $\epsilon 4$ altered whole-brain EIR trajectories. Cartoon depiction of rsSC functional excitatory (red) and inhibitory (blue) connections and formula to calculate EIR. Significant 3-way interaction between sex, *APOE*- $\epsilon 4$, and "time since first scan" ($n = 106$, $\beta = -0.045$, $p = 0.018$). EIR trajectories split by $\epsilon 4$ - (left) and $\epsilon 4$ + (right) as well as male (dark grey) and female (orange). Shaded areas around trend lines represent 95% confidence intervals.

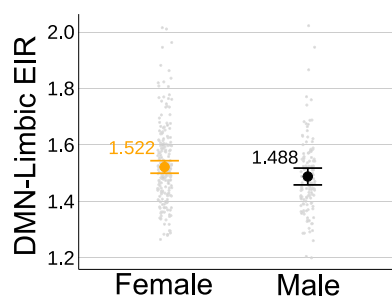


Fig. 3 | Sex altered baseline EIR for DMN-Limbic functional network. Longitudinal results (≥ 3 scans/participant) showing hyperexcitation in the Default Mode Network (DMN) and limbic system of cognitively unimpaired females compared to males ($n = 106$, $p = 0.02$). Values represent marginal means and error bars represent 95% confidence intervals. Regions include middle temporal gyrus, frontal medial cortex, subcallosal cortex, angular gyrus, cingulate gyrus (posterior division), precuneus cortex, parahippocampal gyrus (anterior division), temporal fusiform cortex, hippocampus, amygdala.

model highlight two significant effects: 1) increased EIR, or hyperexcitation, in females at baseline ($b = -0.043$, $p = 0.02$) seen in Fig. 3; 2) decreased EIR with time since first scan ($b = -0.023$, $p = 0.039$). Values in Fig. 3 represent marginal means, reflecting group-level differences between females and males while controlling for additional covariates (e.g., age at first scan).

Interestingly and in contrast to the global EIR results, the sex-based effect reported here in the DMN-limbic functional network showed no strong evidence of moderation by binary *APOE*- $\epsilon 4$ status ($b = 0.018$, $p = 0.635$) or with time since first scan ($b = 0.014$, $p = 0.430$).

Discussion

Decades of research support sex and *APOE*- $\epsilon 4$ as risk factors for AD dementia and amyloid- β burden. Improved neuroimaging has linked macroscale functional and structural changes to AD and amyloid burden. Expanding upon our previous cross-sectional studies^{74,75}, this longitudinal study analyzed excitation-inhibition ratios (EIR) in 106 participants using functional and structural connectivity techniques to identify whole-brain EIR trajectory changes based on sex and *APOE*- $\epsilon 4$ status.

Our analysis suggests that $\epsilon 4$ -positive females are at higher risk of a global hyperexcitable connectivity trajectory than $\epsilon 4$ -negative females and $\epsilon 4$ -positive males. The three-way interaction effect was robust against the confounding factor of amyloid status when included as a non-interacting covariate. Sensitivity analysis supports that global whole-brain hyperexcitation trajectories are a gradual, long-term change. Furthermore, hypothesis-driven DMN-limbic findings bolster our overarching conclusion that cognitively unimpaired females possess a heightened susceptibility to hyperexcitation. In particular, limbic regions (e.g., hippocampus, parahippocampal gyrus, amygdala) and canonical DMN nodes (e.g., precuneus, angular gyrus) showed some of the largest effect sizes in favor of a female-specific hyperexcitable pattern. Taken together, these DMN-limbic results, in conjunction with our whole-brain EIR findings, suggest that even in the absence of clinical impairment, female sex confers a higher “baseline” level of excitatory tone.

These results support a sex-dependent early whole-brain hyperexcitable trajectory in cognitively unimpaired $\epsilon 4$ -positive females. This is corroborated by our previous work that investigated neuropsychiatric testing differences by EIR^{74,75}. Several female specific relationships, were found between EIR and several measures of cognition, including neuropsychiatric testing (logical memory 1 and 2, animals category fluency test, and trail making tests A and B)⁷⁴ and a virtual Morris Water Taks (vMWT)⁷⁵. Given that two-thirds of AD dementia cases are females and that current treatments do not target sex-dependent pathophysiology, our findings suggest a need for novel therapeutics targeting female $\epsilon 4$ -carriers. Indeed, while current monoclonal antibody treatment shows promise, trial results suggest a possible attenuated effect for women and an increased risk

for amyloid-related imaging abnormalities (ARIA) for *APOE*- $\epsilon 4$ carriers^{76,77}. Our results provide a foundation for future studies to understand the interplay between sex and *APOE*- $\epsilon 4$ in guiding drug development for AD-related cognitive impairment. Future studies should test antiepileptic treatment efficacy specifically in female $\epsilon 4$ -carriers.

Limitations of this study include low sample size ($n = 106$), simplifications of genetic *APOE* risk groups, low representation of cognitively impaired participants, and limited amyloid PET data. We binarized $\epsilon 4$ -carrier status due to sample size limitations. Furthermore, there was an imbalance in certain group counts, such as female to male (65: 41) and *APOE*- $\epsilon 4$ carriers to non *APOE*- $\epsilon 4$ (29: 77). The greater representation of *APOE*- $\epsilon 4$ carriers was consistent for males and females. However, while this imbalance exists which limits our sensitivity, power and generalizability; it does not necessarily affect our bias if an appropriate statistical model is chosen. Accordingly, we properly applied linear mixed models which are well-suited for handling unbalanced data and the inclusion of these unbalanced covariates ensures that estimates remain unbiased despite the group size differences. In the future, pseudo-continuous metrics based on pathology-defined AD diagnosis risk, like the *APOE*-npscore, could account for all allele combinations⁷⁸. Although neither the amyloid-negative model nor amyloid as an interacting covariate model showed significant effects, this is likely due to limited data and power (e.g., only 6 *APOE*- $\epsilon 4$ carriers in the amyloid-negative model and very small numbers of amyloid positive). Another limitation was the observed loss of significance for our sensitivity analysis removing two participants with long-term longitudinal data, albeit with little change in effect size and no change in direction. While this may limit the generalizability to observe short term changes in E/I imbalance, this also further supports the idea that global E/I balance changes occur over long and gradual periods of time, concordant with observed cognitive changes. Future studies should increase the sample size and diversity of *APOE*-genetic combinations, amyloid status, and cognitive status. Regional analysis of amyloid would help characterize the theorized proximity-dependent amyloid effect on E/I, seen in humans and mice.

While the Ising model has provided valuable insights into the collective behavior of neuronal populations in our study, it is important to acknowledge its limitations. The model’s binary representation of neuronal states simplifies the complex, continuous nature of neuronal activity and may overlook subtleties associated with graded responses and synaptic integration. This simplification raises the question of whether alternative models could offer a more nuanced understanding of neural dynamics. Indeed, our previous work integrating the rsSC with the Kuramoto model showed excellent reconstruction of brain functional and structural connectivity and needs to be further explored biologically⁶³.

Phenomenological models like the Kuramoto model⁷⁹ and the Hopf normal form model⁸⁰ allow for continuous states and phase relationships between oscillators, potentially capturing synchronization phenomena more effectively. Intermediate models such as the Wilson-Cowan model and neural mass models incorporate average firing rates and synaptic interactions, offering a balance between simplicity and biological relevance. Biophysical models, including the thalamocortical model, delve into the specifics of ionic currents and membrane dynamics, providing a detailed representation of neuronal processes at the cost of increased complexity. Several great reviews have been dedicated to the explanation of how these models work and their trade-offs that we refer the reader to^{24,81,82}.

The use of models that accommodate the full continuum of neuronal activity could enhance the robustness of our findings. Future work should consider integrating these alternative modeling approaches to address the limitations of the current study. By comparing results across models with varying degrees of biological detail, we can better understand the trade-offs involved and potentially uncover more comprehensive insights into neural network dynamics, particularly excitation-inhibition balance.

Moreover, we recognize that structural connectivity estimates, shaped by diffusion-weighted imaging (DWI) preprocessing pipelines, can influence the stability and accuracy of inferred E/I balance. To mitigate these effects, our linear mixed modeling framework includes random intercepts,

effectively accounting for within-subject variability. Additionally, the maximum pseudolikelihood procedure underlying our structurally regularized Ising model stably converges rapidly (Supplementary Fig. 2), demonstrating the stability of rsSC under varying parameter combinations. Future work dedicated to empirically testing the generalizability of these results across many different preprocessing and processing pipelines would benefit the generalizability of EIR and other connectivity-based estimates.

Future E/I balance analysis would benefit from further method development and validation with cell and animal models. While we presented broad-band resting-state EIR, frequency band-specific (with EEG or MEG) resting-state EIR or task-based EIR could be clinically or mechanistically informative, corroborating existing methods showing neural oscillatory changes in MCI and AD^{11,17,18,20–22}. Validating macroscale observations with anatomical and molecular findings in cell and animal models is essential to clarify the interplay between macroscale and microscale E/I observations. Examining how macroscale E/I connectivity correlates with neuron firing rates, myelin and axonal thickness, number of axons in neural tracts, ion channel types and abundance, and neuron type is needed to understand the biology leading to E/I dysfunction, as well as optimize future treatment approaches.

A small but accumulating literature suggests that measuring E/I dynamics in vivo could inform the development of AD symptoms, including progressive loss of cognitive function and behavioral changes. Distinguishing macroscale vs. microscale, functional activity vs. structurally informed functional connectivity, and whole-brain vs. regional metrics will be crucial to moving this field forward. The macroscale hybrid whole-brain structurally informed functional connectivity metric, EIR, holds promise in guiding novel therapeutics that aim to normalize E/I imbalances (e.g., antiepileptic therapies) in AD and providing mechanistic understanding for many electro-abnormal neuropsychiatric disorders.

Methods

Participants

We used data taken with participant consent from OASIS-3 (see acknowledgements). All ethical regulations relevant to human research participants were followed. Analyzed participants ($n=106$) had at least one clinical dementia rating (CDR) of 0, *APOE* genotyping, and three or more resting-state fMRI and DWI scans. In our study, the majority of participants were cognitively unimpaired across 349 total scan events (324 with CDR = 0). We included 22 participants who had scan events with higher CDR scores (21 with CDR = 0.5 and 1 with CDR = 1) because each had at least one scan event with a CDR of 0. This inclusion allowed us to model the trajectory of neural excitation-inhibition across the full preclinical cognitive continuum, up to early mild cognitive impairment. Variability in CDR assessments can lead to temporary increases in scores; participants may score a CDR = 0.5 at one visit but return to CDR = 0 at the next. These transient changes may represent early cognitive fluctuations or assessment variability. Including these participants provides a more accurate and comprehensive modeling of the preclinical continuum. A detailed count of CDR measurements per participant is available in Supplementary Table 13. Whole-brain amyloid PET data for exploratory sub-analysis was included, if available.

MRI preprocessing and analysis

T1-weighted anatomical scans underwent automatic “skull-stripping,” extra-cerebral tissue removal, visual inspection, and intensity inhomogeneity normalization.

Raw fMRI scans underwent first-scan alignment and unwarping, slice-timing correction, outlier identification, segmentation and normalization with T1 images to MNI space, functional smoothing, and regressing out confound effects. Then, to build resting-state structural connectomes (rsSC) for EIR calculation, functional connectomes were computed using Pearson correlations between preprocessed BOLD signal time series of all 105 regions of interest (ROIs), excluding brain stem and cerebellar regions.

Diffusion-weighted MRI (DWI) data underwent head motion and eddy current distortion correction, b_0 alignment, non-brain tissue removal,

fractional anisotropy (FA) map construction, linear registration with participant’s ROI atlas-mapped T1-weighted MRI, and probabilistic tractography to compute structural connectomes (SC) with regional ROI parcellation. Each symmetric SC matrix was normalized by its maximum value for participant-to-participant comparison.

PET imaging included both [11 C]-Pittsburgh compound B and Florbetapir ([18 F]-AV45) with processing steps found in the OASIS data dictionary (<https://www.oasis-brains.org/>). Global amyloid burden was calculated by the mean cortical Standard Uptake Value Ratio with regional spread function (SUVR rsf) from the precuneus, prefrontal cortex, gyrus rectus, and lateral temporal regions. Positive amyloid- β PET scans were defined as having a mean cortical SUVR rsf greater than 1.42 for [11 C]-Pittsburgh compound B PET or 1.19 for Florbetapir PET.

For more detailed information on preprocessing and analysis steps, please consult “Supplementary material.”

Multimodal connectomics and EIR calculation

The resting-state Structural Connectome (rsSC) is a hybrid connectome where connectivity coefficients represent the strength and sign (positive for excitatory, negative for inhibitory) of connections between brain regions (Fig. 4D). It combines multimodal neuroimaging data by fitting an inverse Ising model using resting-state fMRI (rs-fMRI) and structural connectivity from diffusion-weighted MRI (DWI).

The Ising model, originally developed in 1924 to represent pairwise interactions of magnetic dipoles (“spins”) in magnetic materials arranged on a lattice^{83–85}, has been generalized over the past century to model other complex systems. The generalization of the Ising model and other similar spin-glass and pairwise maximum entropy models has been extended to brain connectomics at the microscale^{86,87} and macroscale^{88–93} level. At its core, the Ising model represents a system using three components:

1. Discrete Units: Elements that take binary values (± 1), representing the state of each unit.
2. Pairwise Interactions: Strengths of interaction between pairs of units.
3. External Noise: Variability introduced to account for unmeasured influences, adding randomness to the system.

In connectomics studies, the Ising model (also known as spin glass or pairwise maximum entropy model) effectively captures functional connectivity phenomena. In our application, we enhance the model with a structural regularization term:

- Units: Binary values represent binarized rs-fMRI signals for each brain region of interest (ROI).
- Pairwise Interactions: Represent structural connectivity strengths between ROIs derived from DWI-based tractography.
- External Noise: Optimized to maximize the correlation of the hybrid connectome with empirical functional and structural connectivity.

Forward and inverse Ising problems. In the forward Ising problem, we start with given connectivity coefficients and simulate the binary states of units by minimizing the system’s energy (Hamiltonian). This minimization is probabilistic, governed by Boltzmann probabilities, and often implemented using Monte Carlo methods like Markov Chain Monte Carlo (MCMC). At each iteration, a unit’s state may flip, and the change is accepted based on the Boltzmann probability, which balances energy minimization and external noise. By simulating numerous iterations, we generate time series of binary states that represent binarized fMRI signals. The simulated functional connectivity can then be compared with empirical functional connectivity to assess the model’s accuracy.

However, relying solely on structural connectivity to simulate functional dynamics is insufficient as SC and FC are not strongly correlated^{94–96}. Therefore, we employ the inverse Ising problem with structural regularization to find an optimal connectivity matrix that aligns with both empirical structural and functional data. This approach addresses cases where regions exhibit high functional connectivity without direct structural connections, which could lead to misinterpretation of excitation-inhibition dynamics.

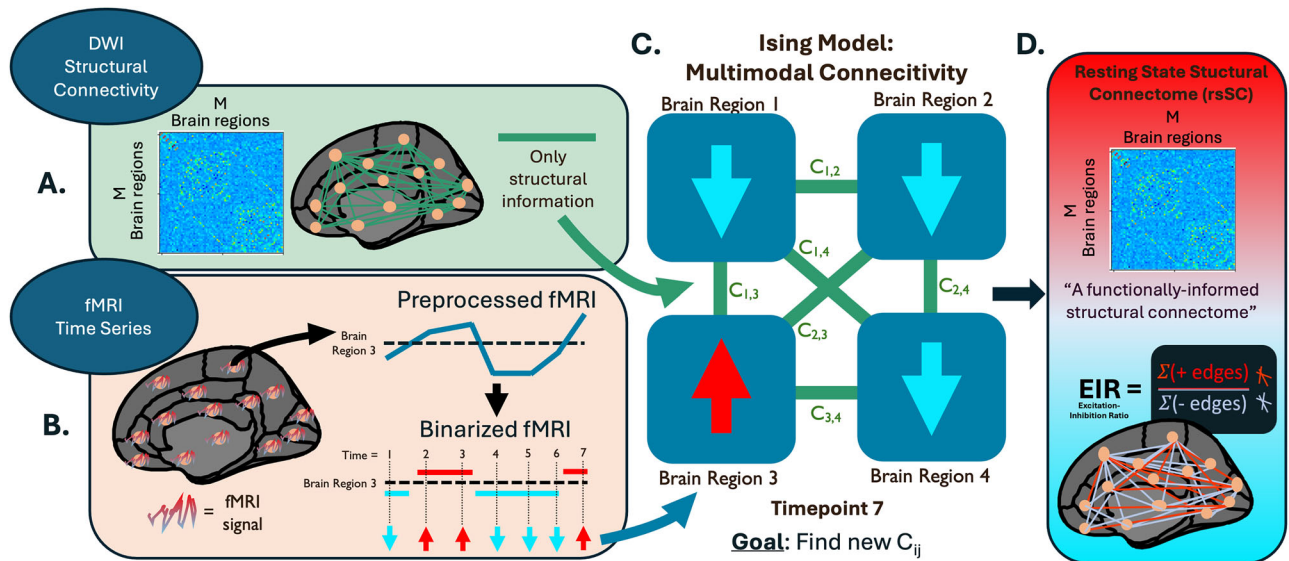


Fig. 4 | Multimodal connectomics model. A structural connectome (A) is generated from DWI, with positive coefficients (C_{ij}) only, and is used to regularize the Ising model (C). Preprocessed fMRI time-series data is binarized (B) and embedded (through a maximum pseudolikelihood function) onto the Ising model as interacting units of brain regions (“spins”). The optimal Ising model embedding results in

functionally-informed structural connectome (D), called the resting-state structural connectome (rsSC), with positive and negative coefficients, which can be inferred as globally excitatory or inhibitory connections, respectively. From the rsSC, we can infer the balance of excitation-inhibition through an excitation-inhibition ratio (EIR).

Our inverse Ising model adjusts the pairwise interaction strengths to fit the empirical functional time series (after binarization) through maximum pseudolikelihood estimation, while the structural regularization term penalizes deviations from empirical structural connectivity. This formulation has two key aspects:

1. Constraint to Empirical Data: Functional activity is constrained by empirical structural connectivity.
2. Allowance for Inhibitory Interactions: The structural constraint is based on the difference between the absolute value of the rsSC and the SC, permitting negative interaction coefficients that resemble inhibitory interactions.

For each set of hyperparameters—structural regularization strength and external noise—we generate a new rsSC.

Optimization of the hyperparameters. To unbiasedly optimize the model’s hyperparameters (structural regularization and external noise), we evaluate how well each rsSC captures both functional and structural brain dynamics. We select the rsSC that maximizes the average of the functional and structural connectivity correlations ($\frac{FC_{correlation} + SC_{correlation}}{2}$):

- Structural Connectivity Correlation: Pearson correlation coefficient between the rsSC and empirical SC.
- Functional Connectivity Correlation: Pearson correlation coefficient between simulated functional connectivity (from the forward Ising problem with rsSC coefficients) and empirical functional connectivity.

The optimization involves:

1. Fitting rsSCs: Generating rsSCs for multiple hyperparameter values using the inverse Ising problem.
2. Measuring FC and SC Correlation: For each rsSC, a functional time series is simulated then correlated with the empirical functional connectivity. Similarly, an SC correlation is calculated directly between the rsSC coefficients and the empirical structural connectivity.
3. Selecting the Best rsSC: Choosing the rsSC that maximizes the average correlation with empirical data.

Interpretation of the rsSC. The optimized rsSC is a network-informed connectivity matrix that best replicates functional and structural

connectivity dynamics. Since functional connectivity is constrained by empirical structural data, we can more confidently infer the net excitation-inhibition tone of connections between ROIs within the network context. A negative connectivity coefficient indicates a net inhibitory influence when functional activity propagates through the network. The global Excitation-Inhibition Ratio (EIR) is calculated as the ratio of summed positive to summed negative connectivity coefficients in each participant’s rsSC. Functional network EIR values are calculated only using connections where at least one node is inside the network.

A methodological overview can be visualized in Fig. 4. For a detailed mathematical treatment and validation of this model, we refer readers to the supplementary text and our previous publications^{62,63}.

Statistics and reproducibility

For this longitudinal data, we used a linear mixed model and started with maximal random effects to minimize bias. Each participant had at least three EIR measurements. We included four fixed effects and their interactions: within-subject (level 1) was time since first scan (in years) and between-subject variables (level 2) included age at first scan, binary *APOE*- $\epsilon 4$ status, and sex. Only cognitively unimpaired participants with at least one CDR of 0 were included. Participants with additional CDR values of 0.5 or 1 represented less than 7% of scan events and were included to capture E/I changes during the transition from cognitively unimpaired to impaired. Due to small sample size limitations, *APOE*- $\epsilon 4$ status and amyloid were binarized as dichotomous variables. The two grand-mean centered time-related variables, age at first scan and time since first scan, were constructed to model EIR trajectory changes over the lifetime and help combat possible polynomial fits. We used random intercepts only due to negligible and non-significant (likelihood ratio test) random slope variance.

Fixed effects and additional contrasts’ p-values were estimated based on degrees-of-freedom calculated using the Kenward-Roger (KR) approximation. Main effects and omnibus interactions were estimated using type III sum-of-squares with KR approximation (“Supplementary material”). We further probed interactions with pairwise contrasts of slopes between sex-*APOE* groups. We also compared an alternative definition of excitation-inhibition to ensure robustness, where instead of forming a ratio, we calculated an excitation percentage of summed positive edges divided by the total sum of all positive and negative edges. All effect sizes are reported as

unstandardized (sex and $\epsilon 4$ status) or semi-standardized coefficients (time since first scan and age at first scan), denoted as b , representing the raw value change in EIR for every binary change (sex and $\epsilon 4$ status) or standard deviation change (time since first scan and age at first scan) of covariate or interaction under evaluation. The unstandardized coefficient was chosen for easier interpretability of raw EIR changes.

Though not in the primary model, whole-brain amyloid status (SUVR) was classified as no PET, amyloid-positive, or amyloid-negative, with three sub-analyses examining amyloid status as a confounder.

Reporting summary

Further information on research design is available in the Nature Portfolio Reporting Summary linked to this article.

Data availability

Analysis code and visualizations are available on GitHub at https://github.com/Drew4495/OASIS_Longitudinal_Analysis_2024. Links to the rsSC modeling code are in the “Supplementary material.” Secondary data sharing is prohibited under OASIS data use agreement but example csv files of the data (including subject and MRI IDs) to be used in the analysis code are provided in order to assist individuals who wish to replicate this analysis with their own data use agreement. Figure 2 example data is in supplementary data 1 and Fig. 3 example data is in supplementary data 2.

Abbreviations

AD	Alzheimer’s Disease
E/I	excitation-inhibition
SEA	subclinical epileptiform activity
rsSC	resting-state structural connectome
KR	Kenward-Roger
ROI	region of interest
FA	fractional anisotropy
CDR	Clinical Dementia Rating

Received: 4 September 2024; Accepted: 3 March 2025;

Published online: 25 March 2025

References

- Barak, O. & Tsodyks, M. Working models of working memory. *Curr. Opin. Neurobiol.* **25**, 20–24 (2014).
- Lim, S. & Goldman, M. S. Balanced cortical microcircuitry for maintaining information in working memory. *Nat. Neurosci.* **16**, 1306–1314 (2013).
- Koolschijn, R. S. et al. Memory recall involves a transient break in excitatory-inhibitory balance. *eLife*. **10**. <https://doi.org/10.7554/eLife.70071> (2021).
- Horvath, A. A. et al. Subclinical epileptiform activity accelerates the progression of Alzheimer’s disease: A long-term EEG study. *Clin. Neurophysiol.* **132**, 1982–1989 (2021).
- Xu, Y. et al. Systematic review of coexistent epileptic seizures and Alzheimer’s disease: Incidence and prevalence. *J. Am. Geriatr. Soc.* **69**, 2011–2020 (2021).
- Fang, Y. et al. Alzheimer Disease and Epilepsy. *Neurology* **101**, e399–e409 (2023).
- Chen, L. et al. The crosstalk between epilepsy and dementia: A systematic review and meta-analysis. *Epilepsy Behav.* **152**, 1–10 (2024).
- Dun, C. et al. Bi-directional associations of epilepsy with dementia and Alzheimer’s disease: a systematic review and meta-analysis of longitudinal studies. *Age Ageing* **51**, afac010 (2022).
- Tai, X. Y. et al. Association of Dementia Risk With Focal Epilepsy and Modifiable Cardiovascular Risk Factors. *JAMA Neurol.* **80**, 445–454 (2023).
- Vossel, K. et al. Effect of Levetiracetam on Cognition in Patients With Alzheimer Disease With and Without Epileptiform Activity: A Randomized Clinical Trial. *JAMA Neurol.* **78**, 1345–1354 (2021).
- Sanchez-Rodriguez, L. M. et al. Personalized whole-brain neural mass models reveal combined A β and tau hyperexcitable influences in Alzheimer’s disease. *Commun. Biol.* **7**, 1–13 (2024).
- Dickerson, B. C. et al. Increased hippocampal activation in mild cognitive impairment compared to normal aging and AD. *Neurology* **65**, 404–411 (2005).
- Bassett, S. S. et al. Familial risk for Alzheimer’s disease alters fMRI activation patterns. *Brain* **129**, 1229–1239 (2006).
- Celone, K. A. et al. Alterations in memory networks in mild cognitive impairment and Alzheimer’s disease: an independent component analysis. *J. Neurosci.* **26**, 10222–10231 (2006).
- Hämäläinen, A. et al. Increased fMRI responses during encoding in mild cognitive impairment. *Neurobiol. Aging* **28**, 1889–1903 (2007).
- Koelewyn, L. et al. Oscillatory hyperactivity and hyperconnectivity in young APOE- $\epsilon 4$ carriers and hypoconnectivity in Alzheimer’s disease. *ELife* **8**, e36011 (2019).
- van Niffterick, A. M. et al. A multiscale brain network model links Alzheimer’s disease-mediated neuronal hyperactivity to large-scale oscillatory slowing. *Alzheimers Res. Ther.* **14**, 101 (2022).
- Wiesman, A. I. et al. Spatially resolved neural slowing predicts impairment and amyloid burden in Alzheimer’s disease. *Brain* **145**, 2177–2189 (2022).
- Engels, M. M. A. et al. Slowing of Hippocampal Activity Correlates with Cognitive Decline in Early Onset Alzheimer’s Disease. An MEG Study with Virtual Electrodes. *Front Hum. Neurosci.* **10**, 238 (2016).
- Nakamura, A. et al. Electromagnetic signatures of the preclinical and prodromal stages of Alzheimer’s disease. *Brain* **141**, 1470–1485 (2018).
- Ochoa, J. F. et al. Precuneus Failures in Subjects of the PSEN1 E280A Family at Risk of Developing Alzheimer’s Disease Detected Using Quantitative Electroencephalography. *J. Alzheimers Dis.* **58**, 1229–1244 (2017).
- van Niffterick, A. M. et al. Resting-state oscillations reveal disturbed excitation-inhibition ratio in Alzheimer’s disease patients. *Sci. Rep.* **13**, 7419 (2023).
- de Haan, W., Mott, K., van Straaten, E. C. W., Scheltens, P. & Stam, C. J. Activity Dependent Degeneration Explains Hub Vulnerability in Alzheimer’s Disease. *PLOS Comput. Biol.* **8**, e1002582 (2012).
- Yang, L. et al. Alzheimer’s Disease: Insights from Large-Scale Brain Dynamics Models. *Brain Sci.* **13**, 1133 (2023).
- Frere, S. & Slutsky, I. Alzheimer’s Disease: From Firing Instability to Homeostasis Network Collapse. *Neuron* **97**, 32–58 (2018).
- Najm, R., Jones, E. A. & Huang, Y. Apolipoprotein E4, inhibitory network dysfunction, and Alzheimer’s disease. *Mol. Neurodegeneration*. **14**, 24 (2019).
- Ribarić, S. Detecting Early Cognitive Decline in Alzheimer’s Disease with Brain Synaptic Structural and Functional Evaluation. *Biomedicines* **11**, 355 (2023).
- Samudra, N., Ranasinghe, K., Kirsch, H., Rankin, K. & Miller, B. Etiology and Clinical Significance of Network Hyperexcitability in Alzheimer’s Disease: Unanswered Questions and Next Steps. *J. Alzheimers Dis.* **92**, 13–27 (2023).
- Targa Dias Anastacio, H., Matosin, N. & Ooi, L. Neuronal hyperexcitability in Alzheimer’s disease: what are the drivers behind this aberrant phenotype? *Transl. Psychiatry* **12**, 1–14 (2022).
- Maestú, F., de Haan, W., Busche, M. A. & DeFelipe, J. Neuronal excitation/inhibition imbalance: core element of a translational perspective on Alzheimer pathophysiology. *Ageing Res. Rev.* **69**, 101372 (2021).
- Busche, M. A. & Konnerth, A. Neuronal hyperactivity – A key defect in Alzheimer’s disease? *BioEssays* **37**, 624–632 (2015).

32. Styr, B. & Slutsky, I. Imbalance between firing homeostasis and synaptic plasticity drives early-phase Alzheimer's disease. *Nat. Neurosci.* **21**, 463–473 (2018).
33. Zott, B., Busche, M. A., Sperling, R. A. & Konnerth, A. What Happens with the Circuit in Alzheimer's Disease in Mice and Humans? *Annu Rev. Neurosci.* **41**, 277–297 (2018).
34. Zott, B. et al. A vicious cycle of β amyloid-dependent neuronal hyperactivation. *Science* **365**, 559–565 (2019).
35. Busche, M. A. et al. Tau impairs neural circuits, dominating amyloid- β effects, in Alzheimer models in vivo. *Nat. Neurosci.* **22**, 57–64 (2019).
36. Busche, M. A. et al. Clusters of hyperactive neurons near amyloid plaques in a mouse model of Alzheimer's disease. *Science* **321**, 1686–1689 (2008).
37. Ren, S. Q. et al. Amyloid β causes excitation/inhibition imbalance through dopamine receptor 1-dependent disruption of fast-spiking GABAergic input in anterior cingulate cortex. *Sci. Rep.* **8**, 302 (2018).
38. Busche, M. A. et al. Critical role of soluble amyloid- β for early hippocampal hyperactivity in a mouse model of Alzheimer's disease. *Proc. Natl. Acad. Sci. USA* **109**, 8740–8745 (2012).
39. Angulo, S. L. et al. Tau and amyloid-related pathologies in the entorhinal cortex have divergent effects in the hippocampal circuit. *Neurobiol. Dis.* **108**, 261–276 (2017).
40. Busche, M. A. Tau suppresses neuronal activity in vivo, even before tangles form. *Brain* **142**, 843–846 (2019).
41. Hall, A. M. et al. Tau-dependent Kv4.2 depletion and dendritic hyperexcitability in a mouse model of Alzheimer's disease. *J. Neurosci.* **35**, 6221–6230 (2015).
42. Hatch, R. J., Wei, Y., Xia, D. & Götz, J. Hyperphosphorylated tau causes reduced hippocampal CA1 excitability by relocating the axon initial segment. *Acta Neuropathol.* **133**, 717–730 (2017).
43. Mucke, L. et al. High-Level Neuronal Expression of A β 1–42 in Wild-Type Human Amyloid Protein Precursor Transgenic Mice: Synaptotoxicity without Plaque Formation. *J. Neurosci.* **20**, 4050–4058 (2000).
44. Hsia, A. Y. et al. Plaque-independent disruption of neural circuits in Alzheimer's disease mouse models. *Proc. Natl. Acad. Sci. USA* **96**, 3228–3233 (1999).
45. Moechars, D. et al. Early phenotypic changes in transgenic mice that overexpress different mutants of amyloid precursor protein in brain. *J. Biol. Chem.* **274**, 6483–6492 (1999).
46. Cirrito, J. R. et al. Synaptic Activity Regulates Interstitial Fluid Amyloid- β Levels In Vivo. *Neuron* **48**, 913–922 (2005).
47. Yuan, P. & Grutzendler, J. Attenuation of β -Amyloid Deposition and Neurotoxicity by Chemogenetic Modulation of Neural Activity. *J. Neurosci.* **36**, 632–641 (2016).
48. Cirrito, J. R. et al. Endocytosis is required for synaptic activity-dependent release of amyloid- β in vivo. *Neuron* **58**, 42 (2008).
49. Nuriel, T. et al. Neuronal hyperactivity due to loss of inhibitory tone in APOE4 mice lacking Alzheimer's disease-like pathology. *Nat. Commun.* **8**, 1464 (2017).
50. Stargardt, A., Swaab, D. F. & Bossers, K. The storm before the quiet: neuronal hyperactivity and A β in the presymptomatic stages of Alzheimer's disease. *Neurobiol. Aging* **36**, 1–11 (2015).
51. Bi, D., Wen, L., Wu, Z. & Shen, Y. GABAergic dysfunction in excitatory and inhibitory (E/I) imbalance drives the pathogenesis of Alzheimer's disease. *Alzheimer's. Dement.* **16**, 1312–1329 (2020).
52. Yamamoto, K. et al. Chronic Optogenetic Activation Augments A β Pathology in a Mouse Model of Alzheimer Disease. *Cell Rep.* **11**, 859–865 (2015).
53. Beam, C. R. et al. Differences Between Women and Men in Incidence Rates of Dementia and Alzheimer's Disease. *J. Alzheimers Dis.* **64**, 1077–1083 (2018).
54. Podcasy, J. L. & Epperson, C. N. Considering sex and gender in Alzheimer disease and other dementias. *Dialogues Clin. Neurosci.* **18**, 437–446 (2016).
55. Koh, M. T., Haberman, R. P., Foti, S., McCown, T. J. & Gallagher, M. Treatment strategies targeting excess hippocampal activity benefit aged rats with cognitive impairment. *Neuropsychopharmacology* **35**, 1016–1025 (2010).
56. Zheng, X. Y. et al. Levetiracetam alleviates cognitive decline in Alzheimer's disease animal model by ameliorating the dysfunction of the neuronal network. *Front. Aging Neurosci.* **14**, 888784 (2022).
57. Mani, V. & Rashed Almutairi, S. Impact of levetiracetam on cognitive impairment, neuroinflammation, oxidative stress, and neuronal apoptosis caused by lipopolysaccharides in rats. *Saudi Pharm. J.* **31**, 101728 (2023).
58. Sanchez, P. E. et al. Levetiracetam suppresses neuronal network dysfunction and reverses synaptic and cognitive deficits in an Alzheimer's disease model. *Proc. Natl. Acad. Sci.* **109**, E2895–E2903 (2012).
59. Bakker, A. et al. Reduction of hippocampal hyperactivity improves cognition in amnesic mild cognitive impairment. *Neuron* **74**, 467–474 (2012).
60. Bakker, A., Albert, M. S., Krauss, G., Speck, C. L. & Gallagher, M. Response of the medial temporal lobe network in amnesic mild cognitive impairment to therapeutic intervention assessed by fMRI and memory task performance. *Neuroimage Clin.* **7**, 688–698 (2015).
61. Cumbo, E. & Lorig, L. D. Levetiracetam, lamotrigine, and phenobarbital in patients with epileptic seizures and Alzheimer's disease. *Epilepsy Behav.* **17**, 461–466 (2010).
62. Fortel, I. et al. Inferring excitation-inhibition dynamics using a maximum entropy model unifying brain structure and function. *Netw. Neurosci.* **6**, 420–444 (2022).
63. Manos, T. et al. Enhanced Simulations of Whole-Brain Dynamics Using Hybrid Resting-State Structural Connectomes. *Neuroscience*. <https://doi.org/10.1101/2023.02.16.528836> (2023).
64. Zhu, D. C., Majumdar, S., Korolev, I. O., Berger, K. L. & Bozoki, A. C. Alzheimer's Disease and Amnesic Mild Cognitive Impairment Weaken Connections Within the Default-Mode Network: A Multi-Modal Imaging Study. *J. Alzheimer's. Dis.* **34**, 969–984 (2013).
65. Dai, Z. et al. Disrupted structural and functional brain networks in Alzheimer's disease. *Neurobiol. Aging* **75**, 71–82 (2019).
66. Hedden, T. et al. Disruption of Functional Connectivity in Clinically Normal Older Adults Harboring Amyloid Burden. *J. Neurosci.* **29**, 12686–12694 (2009).
67. Buckner, R. L. et al. Molecular, Structural, and Functional Characterization of Alzheimer's Disease: Evidence for a Relationship between Default Activity, Amyloid, and Memory. *J. Neurosci.* **25**, 7709–7717 (2005).
68. Supekar, K., Menon, V., Rubin, D., Musen, M. & Greicius, M. D. Network Analysis of Intrinsic Functional Brain Connectivity in Alzheimer's Disease. *PLOS Comput. Biol.* **4**, e1000100 (2008).
69. Gili, T. et al. Regional brain atrophy and functional disconnection across Alzheimer's disease evolution. *J. Neurol. Neurosurg. Psychiatry* **82**, 58–66 (2011).
70. Mormino, E. C. et al. Relationships between Beta-Amyloid and Functional Connectivity in Different Components of the Default Mode Network in Aging. *Cereb. Cortex* **21**, 2399–2407 (2011).
71. Buckner, R. L., Andrews-Hanna, J. R. & Schacter, D. L. The Brain's Default Network. *Ann. N. Y. Acad. Sci.* **1124**, 1–38 (2008).
72. Badhwar, A. et al. Resting-state network dysfunction in Alzheimer's disease: A systematic review and meta-analysis. *Alzheimer's. Dement.: Diagnosis, Assess. Dis. Monit.* **8**, 73–85 (2017).
73. Jiang, X. et al. Altered limbic functional connectivity in individuals with subjective cognitive decline: Converging and diverging findings across Chinese and German cohorts. *Alzheimer's. Dement.* **19**, 4922–4934 (2023).
74. Fortel, I. et al. Disrupted Excitation-Inhibition Balance in Cognitively Normal Individuals at Risk of Alzheimer's Disease. *JAD.* **95**, 1–19 (2023).

75. Fortel, I. et al. Connectome Signatures of Hyperexcitation in Cognitively Intact Middle-Aged Female APOE-ε4 Carriers. *Cereb. Cortex*. **30**, 6350–6362 (2020).
76. Kurkinen, M. Lecanemab (Leqembi) is not the right drug for patients with Alzheimer's disease. *Adv. Clin. Exp. Med.* **32**, 943–947 (2023).
77. van Dyck, C. H. et al. Lecanemab in Early Alzheimer's Disease. *N. Engl. J. Med.* **388**, 9–21 (2023).
78. Deming, Y. et al. Neuropathology-based APOE genetic risk score better quantifies Alzheimer's risk. *Alzheimer's. Dement.* **19**, 3406–3416 (2023).
79. Ódor, G. & Kelling, J. Critical synchronization dynamics of the Kuramoto model on connectome and small world graphs. *Sci. Rep.* **9**, 19621 (2019).
80. Ponce-Alvarez, A. & Deco, G. The Hopf whole-brain model and its linear approximation. *Sci. Rep.* **14**, 2615 (2024).
81. Breakspear, M. Dynamic models of large-scale brain activity. *Nat. Neurosci.* **20**, 340–352 (2017).
82. Pathak, A., Roy D. & Banerjee A. Whole-Brain Network Models: From Physics to Bedside. *Front. Comput. Neurosci.* **16**. <https://doi.org/10.3389/fncom.2022.866517> (2022).
83. Duminil-Copin H. 100 Years of the (Critical) Ising Model on the Hypercubic Lattice. Published online August 1, 2022. Accessed November 20, 2024. <http://arxiv.org/abs/2208.00864>.
84. Budrikis, Z. 100 years of the Ising model. *Nat. Rev. Phys.* **6**, 530–530 (2024).
85. Taroni, A. 90 years of the Ising model. *Nat. Phys.* **11**, 997–997 (2015).
86. Kadirvelu, B., Hayashi, Y. & Nasuto, S. J. Inferring structural connectivity using Ising couplings in models of neuronal networks. *Sci. Rep.* **7**, 8156 (2017).
87. Tkačik, G. et al. The simplest maximum entropy model for collective behavior in a neural network. *J. Stat. Mech.* **2013**, P03011 (2013).
88. Ezaki, T., Watanabe, T., Ohzeki, M. & Masuda, N. Energy landscape analysis of neuroimaging data. *Philos. Trans. R. Soc. A: Math. Phys. Eng. Sci.* **375**, 20160287 (2017).
89. Marinazzo, D. et al. Information Transfer and Criticality in the Ising Model on the Human Connectome. *PLOS One* **9**, e93616 (2014).
90. Nghiem, T. A., Telenczuk, B., Marre, O., Destexhe, A. & Ferrari, U. Maximum-entropy models reveal the excitatory and inhibitory correlation structures in cortical neuronal activity. *Phys. Rev. E*. **98**, 012402 (2018).
91. Niu, W., Huang, X., Xu, K., Jiang, T. & Yu, S. Pairwise Interactions among Brain Regions Organize Large-Scale Functional Connectivity during Execution of Various Tasks. *Neuroscience* **412**, 190–206 (2019).
92. Nuzzi, D., Pellicoro, M., Angelini, L., Marinazzo, D. & Stramaglia, S. Synergistic information in a dynamical model implemented on the human structural connectome reveals spatially distinct associations with age. *Netw. Neurosci.* **4**, 910–924 (2020).
93. Schneidman, E., Berry, M. J., Segev, R. & Bialek, W. Weak pairwise correlations imply strongly correlated network states in a neural population. *Nature* **440**, 1007–1012 (2006).
94. Liégeois, R., Santos, A., Matta, V., Van De Ville, D. & Sayed, A. H. Revisiting correlation-based functional connectivity and its relationship with structural connectivity. *Netw. Neurosci.* **4**, 1235–1251 (2020).
95. Fjell, A. M. et al. Relationship between structural and functional connectivity change across the adult lifespan: A longitudinal investigation. *Hum. Brain Mapp.* **38**, 561–573 (2016).
96. Schulz, M., Petersen M., Cheng B. & Thomalla G. Association of structural connectivity with functional brain network segregation in a middle-aged to elderly population. *Front. Aging Neurosci.* 2024;16. <https://doi.org/10.3389/fnagi.2024.1291162>.

Acknowledgements

The MRI and PET data that support the findings of this study are available in OASIS with the identifier(s) (<https://doi.org/10.1101/2019.12.13.19014902>) [39]. OASIS-3: Longitudinal Multimodal Neuroimaging: Principal Investigators: T. Benzinger, D. Marcus, J. Morris; NIH P30 AG066444, P50 AG00561, P30

NS09857781, P01 AG026276, P01 AG003991, R01 AG043434, UL1 TR000448, R01 EB009352. AV-45 doses were provided by Avid Radio-pharmaceuticals, a wholly owned subsidiary of Eli Lilly. OASIS-3 data are openly available to the scientific community at <https://www.oasisbrains.org>. Thank you to Monica Duran for assistance with the visualization of Fig. 1.

Author contributions

Andrew P Burns: conceptualization (lead), data curation (lead), formal analysis (lead), investigation (lead), methodology (supporting), project administration (lead), software (lead), visualization (lead), writing – original draft preparation (lead), writing – review & editing (lead); Igor Fortel: data curation (supporting), investigation (supporting), methodology (lead), software (supporting), writing – review & editing (supporting); Liang Zhan: funding acquisition, investigation (supporting), methodology (supporting), supervision; Orly Lazarov: funding acquisition, supervision; R. Scott Mackin: supervision, writing – review & editing (supporting); Alexander P Demos: investigation (supporting), methodology (supporting), writing – review & editing (supporting); Barbara Bendlin: funding acquisition, resources, supervision, writing – review & editing (supporting); and Alex Leow: conceptualization (supporting), funding acquisition, methodology (supporting), project administration (supporting), resources, supervision, writing – review & editing (supporting).

Competing interests

The authors declare the following competing interests: Dr. Alex Leow is a cofounder of KeyWise and a scientific advisor to Buoy health and OTSUKA US. All other authors declare no competing interests.

Additional information

Supplementary information The online version contains supplementary material available at <https://doi.org/10.1038/s42003-025-07876-5>.

Correspondence and requests for materials should be addressed to Andrew P. Burns or Alex Leow.

Peer review information *Communications Biology* thanks Pew-Thian Yap and the other, anonymous, reviewer(s) for their contribution to the peer review of this work. Primary Handling Editors: Enzo Tagliazucchi and Benjamin Bessieres. A peer review file is available.

Reprints and permissions information is available at <http://www.nature.com/reprints>

Publisher's note Springer Nature remains neutral with regard to jurisdictional claims in published maps and institutional affiliations.

Open Access This article is licensed under a Creative Commons Attribution-NonCommercial-NoDerivatives 4.0 International License, which permits any non-commercial use, sharing, distribution and reproduction in any medium or format, as long as you give appropriate credit to the original author(s) and the source, provide a link to the Creative Commons licence, and indicate if you modified the licensed material. You do not have permission under this licence to share adapted material derived from this article or parts of it. The images or other third party material in this article are included in the article's Creative Commons licence, unless indicated otherwise in a credit line to the material. If material is not included in the article's Creative Commons licence and your intended use is not permitted by statutory regulation or exceeds the permitted use, you will need to obtain permission directly from the copyright holder. To view a copy of this licence, visit <http://creativecommons.org/licenses/by-nc-nd/4.0/>.

© The Author(s) 2025